A&A, 701, A298 (2025)
https://doi.org/10.1051/0004-6361/202555071

Astronomy & Astrophysics

Extended multi-phase gas reservoirs in the z = 4.3 protocluster SPT2349-56: Non-stellar ionisation sources?

Kevin C. Harrington[1,2,3,4,⋆], Amit Vishwas[5], Allison W. S. Man[6], Carlos De Breuck[7], Padelis P. Papadopoulos[8,9,7,10], Paola Andreani[7], and Thomas. G. Bisbas[11]

[1] Joint ALMA Observatory, Alonso de Córdova 3107, Vitacura, Casilla 19001, Santiago de Chile, Chile
[2] National Astronomical Observatory of Japan, Los Abedules 3085 Oficina 701, Vitacura 763 0414, Santiago, Chile
[3] European Southern Observatory, Alonso de Córdova 3107, Vitacura, Casilla 19001, Santiago de Chile, Chile
[4] Instituto de Estudios Astrofísicos, Facultad de Ingeniería y 455 Ciencias, Universidad Diego Portales, Av. Ejército Libertador 441, Santiago, Chile
[5] Cornell Center for Astrophysics and Planetary Sciences, Cornell University, Ithaca, NY, 14853, USA
[6] Department of Physics & Astronomy, University of British Columbia, 6224 Agricultural Road, Vancouver BC, V6T 1Z1, Canada
[7] European Southern Observatory, Karl-Schwarzschild-Strasse 2, 85748 Garching, Germany
[8] Department of Physics, Section of Astrophysics, Astronomy and Mechanics, Aristotle University of Thessaloniki, 54124 Thessaloniki, Greece
[9] Research Center for Astronomy, Academy of Athens, Soranou Efesiou 4, 11527 Athens, Greece
[10] Max Planck Institute für Astrophysik, Karl-Schwarzschild-Strasse 1, 85748 Garching, Germany
[11] Research Center for Astronomical Computing, Zhejiang Laboratory, Hangzhou, 311000, China

Received 7 April 2025 / Accepted 28 July 2025

ABSTRACT

We aim to characterise the multi-phase gas in the SPT2349-56 protocluster at $z = 4.3$, which is known to host one of the most starbursting and Active Galactic Nuclei (AGN)-rich high redshift environments. For this purpose, we conducted Atacama Pathfinder EXperiment (APEX) single-dish observations of the [C II] 158 μm (hereafter [C II]) line towards the core and north components, which were previously imaged with the Atacama Large Millimeter/submillimeter Array (ALMA). We also present the first [O III] 88 μm (hereafter [O III]) line observations in such a high-redshift protocluster system. We obtain a [C II] line luminosity approximately 1.7 times greater than that recovered by ALMA towards the core, while we recover four times more [C II] line emission than that found in deep ALMA images towards the north component. This suggests that the most massive gas reservoirs lie in the less extreme regions of this protocluster system. A minimum ionised gas mass of $M_{min}(H^+) \sim 3.7 \times 10^{10}$ $M_\odot$ is deduced from the [O III] line, which amounts to 30% of the molecular gas mass in the same area, indicating that a full map of the cluster is necessary for determining the large-scale value. Finally, we obtain star formation rate (SFR) estimates using the [O III] line luminosity and the corresponding ionised gas mass. These yield values that can surpass the far-infrared (IR) continuum-derived SFR under the assumption of a standard stellar Initial Mass Function (IMF), which can be reconciled only if non-stellar ionising sources contribute to the [O III] line luminosity, or if a top-heavy stellar IMF produces a larger fraction of O stars per total stellar mass. This is a distinct possibility in high-energy-particle (HEP)-dominated, rather than UV-photon-dominated, environments in clusters. Future work using far-IR fine-structure and molecular or neutral-atomic lines is necessary to determine the thermal and ionisation states of the multi-phase medium in this protocluster, to understand their maintenance, and to resolve the apparent SFR discrepancy. These line ratios must be measured over a wide range of spatial scales, from individual galaxies up to circumgalactic medium (CGM) and intracluster medium (ICM) scales, which ultimately requires combining wide-field single-dish and high-resolution interferometric observations of such lines in protocluster environments where HEP- and UV-dominated ISM phases can co-exist.

Key words. stars: massive – galaxies: clusters: general – galaxies: high-redshift – galaxies: star formation – submillimeter: ISM

1. Introduction

Distant protoclusters, which are the precursors to modern-day galaxy clusters, are unique laboratories for cosmological structure formation and galaxy evolution across cosmic time (Overzier 2016; Alberts & Noble 2022). Galaxy assembly and star formation, both in situ (within galaxies) and ex situ (within dark matter haloes but beyond the luminous extent of galaxies), in protoclusters require mechanisms to effectively cool the gas and aid its gravitational collapse. Importantly, unlike the interstellar medium (ISM) within galaxies, the thermal or ionisation states of the intracluster medium (ICM) and circumgalactic medium (CGM) gas phases in clusters may not be far-UV radiation-controlled but may instead be dominated by high energy particles (HEPs) (Ferland et al. 2008, 2009; Lim et al. 2017). Unfortunately, in such HEP-dominated environments, where CO, the main tracer of H_2, can be effectively destroyed, yielding [C I] and [C II]-rich gas phases (Bisbas et al. 2015, 2017, 2021, 2025). In these conditions, CO marks only denser sub-regions, which are surrounded by otherwise CO-poor, ([C I]/[C II])-rich H_2 gas reservoirs (Papadopoulos et al. 2018). A CGM H_2 gas reservoir that is C-rich (but relatively CO-poor), with an extent of ≈50 kpc, has already been identified in the protocluster around the Spiderweb galaxy at $z = 2.2$

⋆ Corresponding author: kevin.harrington@alma.cl

(see e.g. Emonts et al. 2018; Chen et al. 2024), requiring long integrations of faint [C I] (1-0) and CO(1-0) line emission. This system was recently confirmed to be embedded in a hot ICM via the Sunyaev Zel'dovich effect (Di Mascolo et al. 2023). Furthermore, cold H_2 gas streams traced by the [C I] (1-0) line emission, extending across 100 kpc, have been shown to fuel 4C 41.17, a massive radio galaxy at $z = 3.8$ (Emonts et al. 2023). Thus, there is a clear need to study the colder (T ~ (20–100) K) gas phase (see e.g. Dannerbauer et al. 2017). This cold phase is expected alongside the warmer (~10^4–10^6 K) ICM-CGM gas in protoclusters, with the former being the readily available fuel for their starburst activity in the early Universe.

Far-IR fine-structure lines can dominate the cooling energy budget within the cold neutral and ionised ISM (see e.g. Spinoglio et al. 2012; Fernández-Ontiveros et al. 2016), with [C II] often considered the dominant coolant, as it traces both neutral and ionised gas (Stacey et al. 2010; Vallini et al. 2015; Gullberg et al. 2015; Lagache et al. 2018; Cormier et al. 2019). Nevertheless, [O III] 88 μm (hereafter [O III]) line emission is often just as bright, while its high ionisation potential (IP) makes it suitable for tracing solely the fully ionised gas phase[1]. In the ISM of galaxies, the [O III] line emission originates from compact (and therefore young) H II regions around massive stars (Cormier et al. 2012; Vallini et al. 2017; Vishwas et al. 2018; Arata et al. 2020). However, such emission has been difficult to observe even at high redshift due to poor atmospheric transmission at its wavelength. Space-based observations of [C II] and [O III] in local metal-poor systems yielded $L_{[O\,III]}/L_{[C\,II]} \sim 1$ (Madden et al. 2013), although such line ratios are difficult to interpret, as the two lines trace vastly different thermal and ionisation states. Indeed, [C II] dominates the cooling budget of the neutral ISM in many local starbursts (De Looze et al. 2014; Díaz-Santos et al. 2017), even as H II regions and a diffuse low-ionisation phase can contribute ~10% to its luminosity in metal-poor ISM. Yet, given the low IP value of neutral carbon (~11.3 eV), it cannot trace the same phase as the [O III] line (~35.1 eV for O^{++}). Indeed, with a higher IP where [O III] is abundant, carbon would not remain in a singly ionised state (the IP for C^+ is ~24.4 eV). Standard photoionisation codes such as CLOUDY (Ferland et al. 2017) naturally yield a multiplicity of thermal and ionisation states within their 1D gas columns, irradiated by stellar or Active Galactic Nuclei (AGN) spectral energy distributions, yet they require more than a single line ratio as input to give any useful results.

Both the [C II] and [O III] lines are accessible to observations in one of the most distant protocluster systems found, namely SPT2349-56 at $z = 4.304$. This protocluster was originally detected in the South Pole Telescope (SPT) 2500 deg^2 millimeter(mm)-survey (Vieira et al. 2010; Mocanu et al. 2013), and spectroscopically confirmed by Strandet et al. (2016) using CO(4-3) and [C II] from the Atacama Pathfinder EXperiment (APEX) telescope after follow-up of the brightest 870 μm detections with the Large APEX BOlometer CAmera (LABOCA; Kreysa et al. 2003; Siringo et al. 2009). The dust continuum maps from LABOCA initially revealed a central source and a northern extension. Subsequent Atacama Large Millimeter/submilleter Array (ALMA) observations identified ~29 CO(4-3)/[C II]emitting objects spread over a few hundred kiloparsecs (proper distance) towards the core and northern extension, with an estimated global star formation rate (SFR) of ~10^4 $M_\odot$ yr^{-1} (Miller et al. 2018; Hill et al. 2020, 2022). Here, we present new [C II] and [O III] observations in SPT2349-56 that are sensitive to large-scale gas distributions in and around the protocluster members, where previous interferometric measurements with ALMA of [C II] in the core and north may have resolved out the corresponding line emission, as suggested by Zhou et al. (2025). We describe the APEX and ALMA measurements in Sect. 2, our results and discussion are presented in Sects. 3 and 4. We provide a brief outlook in Sect. 5 that further motivates the need for sensitive single-dish measurements to study such protocluster systems at high redshift. Throughout this work, we adopt a standard ΛCDM cosmology: $H_0 = 70\,\mathrm{km\,s^{-1}\,Mpc^{-1}}$, $\Omega_m = 0.3$ and $\Omega_\Lambda = 0.7$.

2. Observations and data reduction

2.1. APEX [C II] and [O III] line measurements

The APEX telescope is a 12-m single-dish telescope located on the Chajnantor Plateau in the Atacama Desert in northern Chile. APEX observations targeted both the [C II] and [O III] emission lines using the known redshift $z = 4.304$ and coordinates, as first reported in Strandet et al. (2016) and Miller et al. (2018). The 'core' pointing in the observations corresponds most closely to object C1 in Hill et al. (2020, Core: RA:23:49:42.65, Dec:−56:38:19.4). We also report novel observations of [C II] line emission from the 'north' system located ~45″ away (north; RA: 23:49:42.53, Dec: −56:37:33.2). Figure 1 shows the APEX full width at half maximum (FWHM) of the primary beam for each pointing, overlaid on the dust continuum emission from ALMA Band 6 (1 mm) measurements (Sect. 2.2) for both the core and north regions. The [O III] 88 μm measurements are the first observations of this fine-structure line in the core. Both lines are observable within favourable atmospheric windows at ~358 GHz and ~640 GHz for each line. The [C II] and [O III] lines were observed with the SEPIA345 (Meledin et al. 2022) and SEPIA660 (Baryshev et al. 2015) instruments[2] respectively, between August 31 and September 6 2024 (Project ID: C-0114.F-9704-2024; PI: K. Harrington), during stable nighttime conditions. Precipitable water vapour (PWV) varied between ~0.5–0.8 mm for SEPIA345 (Meledin et al. 2022), the single-pixel, dual-polarisation, 2-sideband (SB; 4-GHz per upper and lower sideband) heterodyne receiver. Excellent observing conditions with PWV < 0.5 mm enabled higher frequency observations with SEPIA660 (Baryshev et al. 2015), which has the same receiver design as SEPIA345. All observations were performed within the APEX control system (Muders et al. 2006), with data recorded using the MPIfR eXtended bandwidth fast Fourier transform spectrometers (FFTS; Klein et al. 2006). Each scan was reduced and analysed using `GILDAS`: Grenoble Image and Line Data Analysis Software[3]. The baseline stability strongly depends on the observed frequency and/or weather conditions. We first subtracted a first-order baseline from the emission line-free channels, guided by the known ~1600 km s^{-1} extent of the line profile (Miller et al. 2018; Hill et al. 2020), at native resolution. We smoothed the baseline-subtracted spectrum before averaging to produce the final spectrum, obtaining a root mean square (RMS) sensitivity of 0.3–0.6 mK (at 90–110 km s^{-1} channel resolution) at ~358 GHz, and 0.3–0.4 mK (at 110–150 km s^{-1}

[1] Excitation potential $E_{ul}/k_B \sim 91$ K and ~163 K, and critical densities of $n_{crit}(H) = 3 \times 10^3$ cm^{-3} (for H I and H_2 as collisional partners) and n(e) = 510 cm^{-3} for the [C II] and [O III] lines, respectively.

[2] APEX Instruments Overview: https://www.apex-telescope.org/ns/observing-run/observing/the-telescope/instruments/

[3] Software information can be found at: http://www.iram.fr/IRAMFR/GILDAS

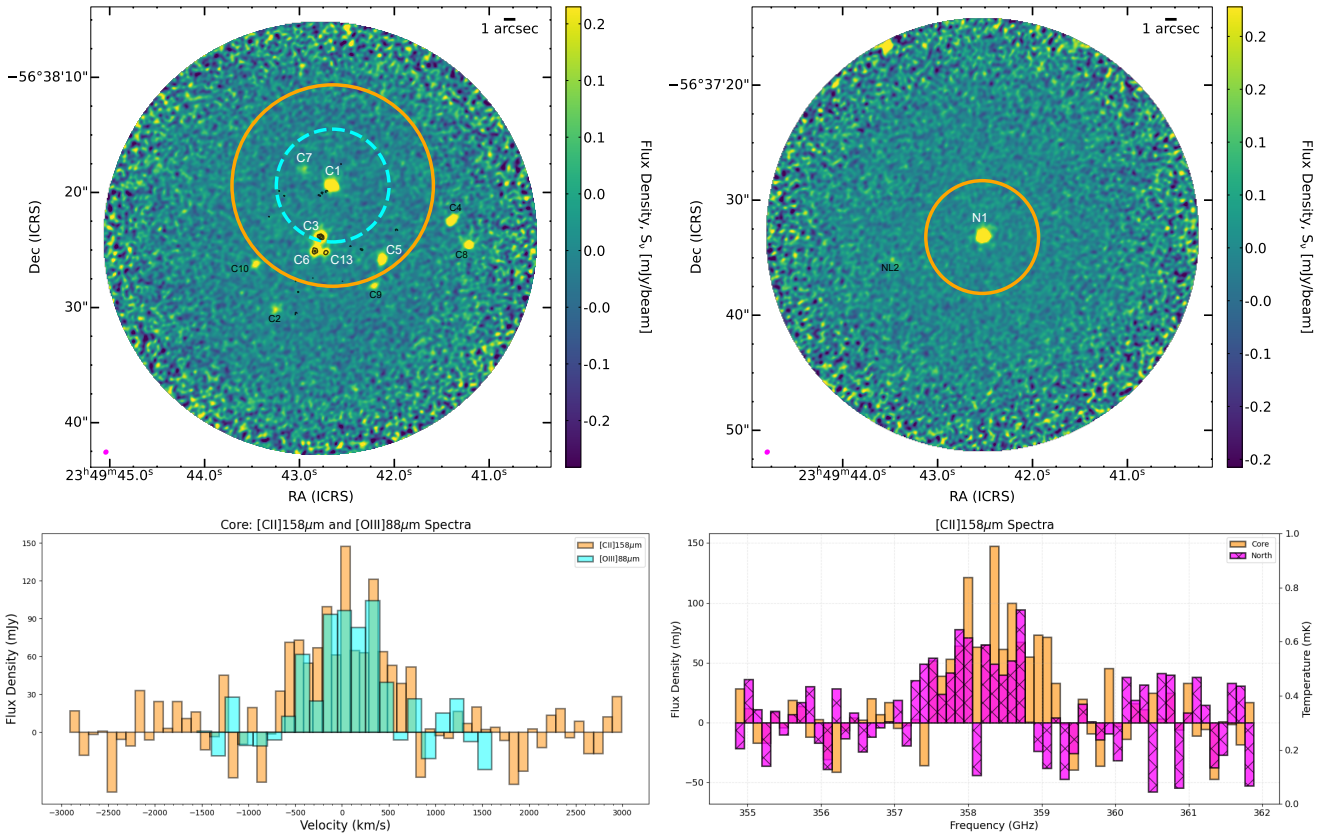

Fig. 1. ALMA Band 6 dust continuum emission from SPT2349-56, showing the core region (top left) and the north extension (top right) 45″ away. The pointing centre and instrument FWHM of APEX SEPIA345 (orange) and SEPIA660 (cyan) observations are overlaid. The Band 6 synthesised beam (magenta) is shown in the bottom-left of each panel. The black contours indicate ALMA Band 10 dust continuum detections towards the core region at signal-to-noise ratio levels of 3, 6, 10, and 15. Several continuum sources are labelled, as identified by Hill et al. (2020). Bottom left: The [C II] (orange; $\delta V = 110\,\mathrm{km\,s^{-1}}$) and [O III] 88 μm (cyan; $\delta V = 140\,\mathrm{km\,s^{-1}}$) spectra (Flux density vs. velocity, corrected using $z = 4.304$). Bottom right: The [C II] spectra (flux density or antenna temperature vs. frequency) shown for both observations of the core (orange; $\delta V = 100\,\mathrm{km\,s^{-1}}$) and north (fuchsia; $\delta V = 100\,\mathrm{km\,s^{-1}}$) fields.

Table 1. APEX single-dish measurements of [C II] and [O III] lines.

Line	Integrated Flux (Jy km s^{-1})	$L_{\rm line}$ (10^{10} L$_\odot$)	$L'_{\rm line}$ (10^{10} K km s^{-1} pc^2)	RMS per 100 km s^{-1} (mK)
[C II] Core	101.7 ± 15.1	6.1 ± 0.9	27.5 ± 4.1	0.38
[O III] Core	78.2 ± 15.6	8.3 ± 1.7	6.6 ± 1.3	0.65
[C II] North	80.4 ± 12.1	4.8 ± 0.7	21.8 ± 3.3	0.3

channel resolution) at ~640 GHz. Using the APEX telescope efficiencies of 46.4 Jy K^{-1} and 59.5 Jy K^{-1} at 358.4 GHz and 639.7 GHz, respectively[4], we scaled to a measured flux density. We then integrated across each line profile to calculate line luminosities (Table 1; e.g. Solomon & Vanden Bout 2005; Carilli & Walter 2013 and references therein for the formalism used). The total uncertainties of around 15–20% arise primarily from the flux calibration, pointing and focus, and baseline subtraction errors.

2.2. ALMA Band 6 and Band 10 dust continuum

In this work, we utilised ALMA dust continuum measurements to identify the protocluster galaxy members with respect to the [C II] and [O III] line emission measurements from APEX detections. Band 10 (Uzawa et al. 2013) dust continuum measurements were recently obtained at 875–900 GHz (PID 2024.1.01465.S; PI: K. Harrington) from ALMA 12-m observations conducted between October 12 and November 6 2024 under excellent conditions: PWV and phase RMS 0.3 mm and <15 μm, respectively. We obtained calibrated measurement sets of the two observations by rerunning the ALMA pipeline on the raw data, using `CASA` (McMullin et al. 2007). We then inspected the pipeline weblog and concluded that sufficient flagging had been applied, before imaging using the `tclean` task in `CASA` with all spectral windows and an auto-multithresh (Kepley et al. 2020) cutoff, resulting in an RMS of approximately 0.7 mJy beam^{-1}. Three objects were detected, with more observational details described in Appendix A (Table A.1). We also used archival ALMA 12-m imaging from observations conducted on September 1 2022 of the core and north in Band 6

[4] https://www.apex-telescope.org/telescope/efficiency/index.php

(PID 2021.1.01313.S; PI: R. Canning). We utilised the pipeline products available from the ALMA archive to plot a continuum image from 223–240 GHz (Fig. 1).

3. Results

3.1. Excess [C II] line emission

The SPT2349-56 protocluster at $z \sim 4.3$ consists of multiple member galaxies concentrated in a northern and southern spatial configuration (Fig. 1, Fig. B.1). The APEX [C II] observation towards the southern region, i.e. the core, suggests that these single-dish measurements capture the [C II] line emission from 19 out of 23 objects presented in deep ALMA 12-m observations ($\sim$0.2 mJy beam^{-1} per 13 km s^{-1} channel resolution) presented in Hill et al. (2020). The sum of the [C II] line fluxes for all 19 objects detected with the ALMA 12-m array, excluding objects 'C2,C4,C8,C19'[5], results in $\int_{\Delta V} S_\nu([C\,II])dV \sim 60$ Jy km s^{-1} (Hill et al. 2020). To evaluate whether ALMA interferometric observations have filtered out extended [C II] beyond the maximum resolvable scale ($\sim$5–6″) and sensitivities probed by both Miller et al. (2018) and Hill et al. (2020), we compared the individual [C II] line fluxes obtained from interferometry and those from single-dish observations of the core. The APEX [C II] measurements (Table 1) indicate a total line flux greater than 100 Jy km s^{-1}, i.e. about 1.7 times the line emission compared to ALMA. Based on the luminosity function discussed in Hill et al. (2020) and comparing the sensitivity of the ALMA observations, we estimate that no more than 10–15% of the excess flux can be attributed to low-luminosity galaxies that are within the (relatively small) beam, but undetected with ALMA.

In addition, we present the first single-dish observation towards the north region (Table 1), centred on object 'N1' as presented in Hill et al. (2020). Our north pointing consists of a single central object in the archival Band 6 continuum and [C II]. Hill et al. (2020) report that this object ('N1') has $\int_{\Delta V} S_\nu([C\,II])dV = 18.9$ Jy km s^{-1}. We measure a [C II] line flux of 80 Jy km s^{-1} from APEX observations, i.e. four times the [C II] line emission measured by deep ALMA observations. Indeedamente, the largest nongalaxy-bound reservoir of [C II]-emitting gas in the SPT2349-56 protocluster lies in the north. Moreover, the north component [C II] emission amounts to nearly 80% of that of the core component, yet it contains only one [C II] line emitter. The combined core and north [C II] line luminosity ($\sim 11 \times 10^{10}$ L$_\odot$) amounts to $\sim$0.14% of the total IR luminosity of the entire protocluster, $L_{IR} \sim 8 \times 10^{13}$ L$_\odot$ (Strandet et al. 2016; Miller et al. 2018; Hill et al. 2020). The factor of 1.7 times the [C II] line emission from the core already indicates the presence of a significant amount of gas (possibly located between these systems) around the core members. Additional faint objects revealed in deep ALMA measurements by Hill et al. (2020) resulted in the detection of multiple new objects and fainter emission surrounding some of the objects within the core (<1 Jy km s^{-1}) that were not originally detectable by Miller et al. (2018). The fainter objects increased the total ALMA-detected [C II] line intensity by only $\sim$10–15 Jy km s^{-1} for the same area covered by APEX. This suggests that the factor of 1.7 increased [C II] emission in the core does not come from the recently detected faint [C II]-emitting systems, but from an ICM-CGM phase, with the excess [C II] emission being even more pronounced in the north component.

[5] These objects are not within the pointing of the primary beam ($\sim$2–3″) of APEX.

3.2. First [O III] 88 μm line detection in a $z > 1$ protocluster

The [O III] 88 μm line was first detected in the early Universe in two composite galaxies with both AGN and starburst activity (Ferkinhoff et al. 2010). In the local Universe, it is thought to be powered solely by O star radiation fields (e.g. Cormier et al. 2012; Lambert-Huyghe et al. 2022 and references therein), even though its critical density ($n_{e,crit} \sim 510$ cm^{-3}) and low excitation potential ($E_{10}/k_B \sim 163$ K) allow it to remain luminous at lower temperatures and densities of ionised gas beyond the immediate vicinity and/or inside young, compact H II regions. Within such regions, this line is insensitive to the much higher local temperatures and is nearly LTE-excited for $n_e \gtrsim 10^3$ cm^{-3}. The [O III] emission in the core has line fluxes and profiles comparable to those of the [C II] line (Figure 1), as observed in other known cases of dusty star-forming galaxies (De Breuck et al. 2019). The [O III] line has a similar luminosity to [C II] despite covering an area roughly three times smaller in the pointing[6] (Figs. 1, A.1), with $L_{[O\,III]}/L_{[C\,II]} = 1.3$ and $L_{[O\,III]} = (8.3 \pm 1.7) \times 10^{10}$ L$_\odot$; yet, as noted in Sect. 1, these two lines trace different gas phases altogether. We can nevertheless use the [O III] frequency-integrated flux density, F_{10}, to obtain the minimum amount of ionised hydrogen gas, given by

$$M_{min}(H^+) = F_{10}\left[\frac{4\pi D_L^2}{(g_1/Z(T_e)\,e^{-E_1/k_B T_e})A_{10}h\nu_{10}}\right]\frac{m_H}{X(O^{++})}, \quad (1)$$

where $n_1 = N_1/N_{tot} = [g_1/Z(T_e)]e^{-E_1/k_B T_e}$ is the occupation number of the upper level (for LTE), $Z(T_e)$ is the three-level partition function, $A_{10} = 2.7 \times 10^{-5}$ s^{-1} is the Einstein coefficient for spontaneous emission, $\nu_{10} = 3393.00624$ GHz is the line frequency, and $X(O^{++})$ is the fractional abundance of oxygen in the doubly ionised state. For hot plasma, $e^{-E_1/(k_B T_e)} = e^{-163/T_{e(K)}} \sim 1$, and for all oxygen atoms in the doubly ionised state (i.e. $X(O^{++}) \sim X(O) = 5.9 \times 10^{-4}$; assumed Milky Way value) we obtain

$$M_{min}(H^+) \sim 2.6 \times 10^{-4} X(O)^{-1}\left(\frac{L_{10}}{L_\odot}\right) M_\odot, \quad (2)$$

where L_{10} the line luminosity, which yields $M_{min}(H^+) \sim 3.7 \times 10^{10}$ M$_\odot$. Sub-thermal line excitation, cooler plasma, optical depth effects reducing the observed [O III] line intensity, or oxygen atoms at a lower ionisation state, will all increase the actual $M(H^+)$. This minimum ionised gas mass already amounts to 30% of the molecular gas masses reported for the sum of all objects within the APEX beam (Hill et al. 2020, see Table 3). The question then arises whether the high [O III] line (and the large implied ionised gas mass) can be explained as the outcome of the total IR-derived SFR for the core. The APEX [O III] observations cover less than a third of the 23 core objects. Estimates of the IR-derived SFR from these objects yields SFR ~ 2500 M$_\odot$ yr^{-1}, while the larger core area within 300 kpc (proper distance), containing all 23 objects, has a total IR-derived SFR of $\sim$5000 M$_\odot$ yr^{-1} (Hill et al. 2020).

4. Discussion

In this section, we discuss the significance of the single-dish [C II] and [O III] line detections. We first derive an independent SFR estimate from the [O III] line luminosity. As mentioned above, the [O III] line typically traces star-forming regions in the

[6] Due to the differences in the beam size between 358 GHz and 640 GHz.

vicinity of intense ionisation sources owing to the requirement of 35.1 eV photons to produce O^{2+}. In deriving this SFR and comparing it with the known IR-derived SFR, we can explore whether the [O III]-deduced SFR is sufficiently high to suggest significant non-stellar contributions to the observed [O III] line luminosity from other sources in or around individual star-forming galaxies within SPT2349-56.

It can be shown that for only stellar types O5.5V or above, produce sufficient ionising flux to keep He doubly ionised (requires 24.6 eV) throughout the Strömgren sphere (e.g. Draine 2011). Therefore, the presence of such stars is essential for attributing the observed [O III] luminosity to star formation activity. First, we estimate the number of representative O5.5 class V stars, whose typical bolometric luminosity is $10^{5.41}\,L_\odot$ (see Table 1 in Martins et al. 2005). Metal lines are the primary coolants of photoionised gas, emitting approximately 1% of the incident bolometric luminosity. Therefore, we adopt $\epsilon_O = 1\%$ to convert the observed [O III] luminosity into the expected bolometric luminosity of the stars responsible for keeping the gas ionised, $L_{[O\,III]}/\epsilon_O = N_{O5.5V} \times L_{O5.5V}$. This results in ~32.3 million O5.5V stars. Using STARBURST99 (Leitherer et al. 1999) stellar population synthesis models, we find that a continuous star formation episode with SFR = $1\,M_\odot\,yr^{-1}$, sustained over 6–8 Myr, results in approximately $10^{4.35}$ O stars. These models count all stars $\gtrsim$15.6 $M_\odot$ as O-stars. Calculating the integral over the IMF used for SB99[7] between $M_{low} = 34.4\,M_\odot$ to $M_{up} = 100\,M_\odot$, yields a fraction of stars O5.5V or greater as $f_{(\%>O5.5V\,M_\odot)} = 28.57\%$. We therefore derive a scaling between an SFR = $1\,M_\odot\,yr^{-1}$ and $N_{O5.5V} = f_{(\%>O5.5V\,M_\odot)} N(\text{O stars}, 1\,M_\odot\,yr^{-1}) \sim 6400$, as expressed by the following independent [O III] 88 μm-derived equation for the SFR, which uses the known properties of O stars and the STARBURST99 models closest to solar metallicity ($Z = 0.02$):

$$\frac{SFR_{O\,III}}{M_\odot\,yr^{-1}} = \frac{L_{O\,III}}{\epsilon_O L_{O5.5V}} \times \frac{1}{f_{(\%>O5.5V\,M_\odot)}\,N_{(\text{O stars},\,1\,M_\odot\,yr^{-1})}}, \quad (3)$$

which gives $SFR_{O\,III} \sim 5050\,M_\odot\,yr^{-1}$, exceeding the $2500\,M_\odot\,yr^{-1}$ value estimated for this area of the protocluster (Hill et al. 2020). The OIII-deduced SFR would be even higher if the assumed metallicity were lower, further exaggerating the discrepancy.

The previous equation demonstrates that the OIII-deduced SFR may be equal to or even exceed the total IR-derived SFR. Therefore, we provide an independent estimate of the formation rate of O stars from the [O III]-deduced H^+ mass reservoir, requiring two assumptions: (a) this reservoir consists solely of young ultra-compact H II (UCHII) regions around O5–O7 stars (those with a high ionisation parameter U sufficient to maintain the O^{++} ionisation state); (b) these stars are replenished in a steady-state manner by an equal mass of molecular gas (copious amounts of which have been detected in this protocluster; (e.g. Zhou et al. 2025)). Using the turbulence-regulated SF theory (Krumholz & McKee 2005), this replenishment occurs by collapsing dense gas cores on timescales $\Delta t_* = f_* \Delta t_{ff} = (f_*/4)\sqrt{3\pi/(2G\langle\rho\rangle)}$, thus:

$$\frac{SFR_{O\,stars}}{M_\odot\,yr^{-1}} \sim \frac{\epsilon_* M_{min}(H^+)}{\Delta t_*} \sim 818 \left(\frac{\epsilon_*}{f_*}\right)\left(\frac{\langle n\rangle}{cm^{-3}}\right)^{1/2}, \quad (4)$$

within the protocluster area sampled by the APEX beam. From turbulence-regulated star formation theory, the parameter $f_* = (SFR_{ff})^{-1}$ ranges from 70–180, where $SFR_{ff} \sim 0.0056$–0.014 is the normalised SFR per free-fall time Δt_{ff} (for core virial parameters of $a_{vir} = 1.3$–5; see Equations (21) and (30) in Krumholz & McKee 2005). Meanwhile, $\epsilon_* = M_O/M_{UCHII}$ represents the O star mass per ionised gas mass of its UCHII region. For molecular cloud core densities of $\langle n\rangle = (1$–$5) \times 10^4\,cm^{-3}$ (typical of dense star-forming molecular gas), and $\epsilon_* \sim 0.65$ (for a UCHII size of r ~ 0.5 pc, using the n_e-(2r) relation from Kim & Koo 2001 (Figure 9), and a mean mass of $M_O = 40\,M_\odot$ for O6–O7 spectral types), we estimate $SFR_{O\,stars} \sim (300$–$1700)\,M_\odot\,yr^{-1}$. This range already accounts for approximately 12–68% of the total, IR-derived SFR computed for this protocluster area assuming a standard stellar IMF. For a lower $X(O^{++}) = [O^{++}/H^+] = 0.3 \times (O) = 1.77 \times 10^{-4}$ abundance inside the H II regions (appropriate for O5.5 stars with H^+ and He^+ throughout their volume)[8] $M(H^+)_{min} \sim 1.2 \times 10^{11}\,M_\odot$, raising the implied $SFR_{O\,stars}$ to $\sim(1000$–$6000)\,M_\odot\,yr^{-1}$, which is at least 65% of and can even exceed the IR-derived total SFR (an obvious impossibility). These two independent arguments that estimate the OIII-deduced SFR suggest possible nonstellar contributions to the observed [O III] line luminosity or a top-heavy stellar IMF (a possible outcome of HEP-dominated ISM; Papadopoulos et al. 2011). These are important issues that will be addressed by future studies and spatially resolved analyses.

The APEX [O III] observations covered the region of the core, encompassing only three of the brightest galaxies initially discovered by Miller et al. (2018) (objects C1, C3, and C7; Hill et al. 2020). Objects C1 (Band 10 undetected) and C3 (Band 10 detected) are among the brightest reported individual [C II] emitters (Miller et al. 2018; Hill et al. 2020). However, C3 is associated with a known radio-loud AGN system composed of C3, C6, and C13, all detected in Band 10 and indicating a strong dust heating source. Subsequent X-ray observations indicate that C1 and C6 host AGN with roughly Compton-thick gas ($N_H \sim 10^{24}\,cm^{-2}$; Chapman et al. 2024; Vito et al. 2024). The contribution of these galaxies to the APEX-observed [O III] luminosity remains uncertain, as does the existence of any extended [O III]-emitting ICM phase within the protocluster. Moreover, the systems detected in the ALMA Band 10 measurements (C3, C6, and C13; Fig. A.1) are dusty starbursts and could have significant optical depths even in the far-IR. Indeed, extreme dusty merger starbursts such as Arp 220 have been found to be optically thick out to 450 μm (Papadopoulos et al. 2010) and even 2.6 mm (Scoville et al. 2017), while the Red Radio Ring, a strongly lensed dusty star-forming galaxy (DSFG) at $z = 2.6$, appears optically thick out to 200 μm (Harrington et al. 2019). Any dust optical depth corrections or low-density ionised gas phase (sub-thermally exciting the [O III] line) in the protocluster would only increase the corresponding $M(H^+)$, thereby complicating its attribution solely to H II regions surrounding O stars (as these are produced by a standard IMF).

Luminosity ratios $L_{O\,III}/L_{C\,II} > 1$ have been observed previously in high-redshift starburst galaxies at $z \sim 6$–9 (Harikane et al. 2020), exceeding values found in local starbursts and dwarf galaxies (Fujimoto et al. 2024 and references therein). In these high-redshift systems, where O-stars appear abundant, we would expect a richer release of O compared to C (which originates from lower-mass, longer-lived stars). This affects the C/O abundance ratio, creating the so-called

[7] https://massivestars.stsci.edu/starburst99/figs/fig38.html

[8] The value 0.3 is representative of the distribution between 0.2 to 0.6 in Figure 14 of Amayo et al. (2021).

α-enhanced ISM. An α-enhanced ISM may also exhibit high $L_{O\,III}/L_{C\,II}$ (Bisbas et al. 2024, 2025); however, it is not clear whether the ISM and ICM power sources are dominated by the star-formation-produced far-UV photons or are HEP-dominated instead. Recently, the environment around a known dusty star-forming galaxy at $z = 2.8$ was imaged by the *James Webb Space Telescope* (*JWST*), revealing 2.5 kpc filamentary structures of [O III] $\lambda\lambda$4959, 5007 line emission extending out to 60 kpc beyond the host system (Peng et al. 2025), precisely tracing the previously imaged Lyman-α emission, indicating a shock-heated CGM. Solimano et al. (2025) report that radiative shocks are insufficient to power the [O III] $\lambda\lambda$4959, 5007 line emission in a $z \sim 4.5$ protocluster, and explored the possibility of outflows and AGN in powering these CGM-scale [O III]. Harikane et al. (2025) have recently analysed both singly and doubly ionised optical and far-IR oxygen lines, suggesting that the far-IR emission lines arise primarily from relatively low-density gas with electron densities around $n_e \sim 100\,\mathrm{cm}^{-3}$. Moreover, far-UV photon-deficient thermal ISM states have been found to dominate large molecular gas reservoirs even within extreme dusty starbursts such as NGC 6240 (Papadopoulos et al. 2014), a distinct possibility also for ICM-CGM in galaxy clusters (Ferland et al. 2008, 2009; Lim et al. 2017). The initial conditions of star formation are strongly impacted by the dominant ISM heating source, which in turn affects the resulting in situ (galaxies) and ex situ (CGM-ICM) stellar IMF that builds up the stellar mass in the Universe.

The significance of the [C II] excess (1.4 times in the core and four times in the north compared with star-forming galaxies) is that it likely traces a diffuse CGM or a preheated proto-ICM, which may play a critical role in sustaining the high SFR observed. The larger [C II] excess in the north region could reflect variations in environmental conditions, but further investigation are needed to clarify its origin (see e.g. Fujimoto et al. 2019). Without spatially resolved observations of these emission lines, we can only speculate, but not definitely confirm, the source of ionising photons at this time, It is assumed that extended [O III] may be less likely than extended [C II], given the higher IP. Previous works have explored the possibility of extended [C II] halos around individual galaxies and merging systems using ALMA (e.g. Fujimoto et al. 2019; Ginolfi et al. 2020), while more recent single-dish observations have revealed even more spatially extended [C II] in protocluster systems (e.g. De Breuck et al. 2022). We provide evidence that [O III], having a much higher IP, exhibits a similar distribution, as inferred from the line width of [C II]. This raises the question of what causes the widespread [O III] line emission. Is widespread star formation enough to explain this, or must alternative mechanisms such as shock-driven excitation and/or widespread AGN activity be invoked, especially considering that there may be higher AGN activity in protoclusters (Vito et al. 2024; Shah et al. 2024), including SPT2349-56? This highlights the critical importance of using reliable ionised and neutral gas phase line ratio diagnostics to determine the thermal and ionisation states in extraordinary systems such as the SPT2349-56 protocluster in the early Universe.

5. Conclusions and outlook

Two new APEX single-dish measurements of the [C II] line in the SPT2349-56 protocluster reveal ~1.7 times the [C II] line emission previously measured with ALMA 12-m observations of the core, while the [C II] detection from the north reveals roughly four times the [C II] line luminosity than detected by deep ALMA 12-m observations. Both results suggest the presence of additional amounts of ICM and/or CGM gas. An APEX [O III] line measurement towards the core revealed the presence of a large reservoir of O^{++}, corresponding to a massive H^+ gas reservoir. The latter is difficult to reconcile solely as the product of star formation in this intensely star-forming protocluster, unless non-stellar sources such as HEPs and/or strong shocks contribute to the CGM and ICM ionisation, or non-standard (top-heavy) stellar IMFs are considered. It is therefore imperative that the multi-phase CGM and/or ICM reservoir in this and other such extraordinary systems be studied both in its ionised and neutral gas phases, using appropriate line ratios reliably measured across scales ranging from individual galaxies up to large-scale CGM and/or ICM distributions. Such studies are impossible with interferometers alone, due to short u-v spacing that filtered out large-scale emission, which biased the assessments of both the true mass of the CGM and ICM components and their thermal and chemical states. Our work demonstrates the necessity of overcoming these short-spacing issues in interferometric data by complimenting them with measurements of far-IR fine-structure lines with single-dish facilities. This further motivates the development of future facilities such as the Atacama Large Aperture Submillimeter Telescope (i.e. AtLAST; Mroczkowski et al. 2025), capable of accessing to the required high-frequency ranges without filtering out extended line emission.

Acknowledgements. The authors would like to pay respects to the passing of German Astronomer, Dr. Karl Menten: https://www.mpifr-bonn.mpg.de/announcements/2025/1. He was the founder of APEX, had an enormous influence in ensuring the development of the Atacama Large Millimeter/submillimeter Array, and has left a scientific legacy for years and years to come. For distinguished people, every sky is a shelter. The authors would like to thank the referee for their thoughtful comments and constructive review. The authors also thank Rob Ivison, Laya Ghodsi, Nick Foo, as well as Dazhi Zhou, Scott Chapman and Nikolaus Sulzenauer, for helpful comments and discussions. We would also like to thank all of the APEX team of operators, observers and staff for making these successful observations, including Juan-Pablo Perez-Beapuis, Manuel Merello, Felipe MacAuliffe, Claudio Agurto, Mauricio Martinez, Francisco Azagra, Pablo Garcia and Macarena Lopez. PPP would like to thank the ESO visitorship program that hosted him in the period November-March 2024–25, as well as Thorsten Naab and Bo Peng at MPA for the hospitality and the intense discussions. This work was supported by the European Southern Observatory through available travel funds for Fellows, which has been greatly appreciated by KCH. AWSM acknowledges the support of the Natural Sciences and Engineering Research Council of Canada (NSERC) through grant reference number RGPIN-2021-03046 and the ESO Visitor Program. The data were collected under the Atacama Pathfinder EXperiment (APEX) Project, led by the Max Planck Institute for Radio Astronomy at the ESO La Silla Paranal Observatory. This paper makes use of the following ALMA data: ADS/JAO.ALMA#2024.0.01465.S. ALMA is a partnership of ESO (representing its member states), NSF (USA) and NINS (Japan), together with NRC (Canada), NSTC and ASIAA (Taiwan), and KASI (Republic of Korea), in cooperation with the Republic of Chile. The Joint ALMA Observatory is operated by ESO, AUI/NRAO and NAOJ. TGB acknowledges support from the Leading Innovation and Entrepreneurship Team of Zhejiang Province of China (Grant No. 2023R01008).

References

Alberts, S., & Noble, A. 2022, Universe, 8, 554
Amayo, A., Delgado-Inglada, G., & Stasińska, G. 2021, MNRAS, 505, 2361
Arata, S., Yajima, H., Nagamine, K., Abe, M., & Khochfar, S. 2020, MNRAS, 498, 5541
Asaki, Y., Maud, L. T., Fomalont, E. B., et al. 2020a, ApJS, 247, 23
Asaki, Y., Maud, L. T., Fomalont, E. B., et al. 2020b, AJ, 160, 59
Asaki, Y., Maud, L. T., Francke, H., et al. 2023, ApJ, 958, 86
Baryshev, A. M., Hesper, R., Mena, F. P., et al. 2015, A&A, 577, A129
Bisbas, T. G., Papadopoulos, P. P., & Viti, S. 2015, ApJ, 803, 37
Bisbas, T. G., van Dishoeck, E. F., Papadopoulos, P. P., et al. 2017, ApJ, 839, 90
Bisbas, T. G., Tan, J. C., & Tanaka, K. E. I. 2021, MNRAS, 502, 2701
Bisbas, T. G., Zhang, Z.-Y., Gjergo, E., et al. 2024, MNRAS, 527, 8886
Bisbas, T. G., Zhang, Z.-Y., Kyrmanidou, M.-C., et al. 2025, A&A, 697, A115

Carilli, C. L., & Walter, F. 2013, ARA&A, 51, 105
Chapman, S. C., Hill, R., Aravena, M., et al. 2024, ApJ, 961, 120
Chen, Z., Dannerbauer, H., Lehnert, M. D., et al. 2024, MNRAS, 527, 8950
Cormier, D., Lebouteiller, V., Madden, S. C., et al. 2012, A&A, 548, A20
Cormier, D., Abel, N. P., Hony, S., et al. 2019, A&A, 626, A23
Dannerbauer, H., Lehnert, M. D., Emonts, B., et al. 2017, A&A, 608, A48
De Breuck, C., Weiß, A., Béthermin, M., et al. 2019, A&A, 631, A167
De Breuck, C., Lundgren, A., Emonts, B., et al. 2022, A&A, 658, L2
De Looze, I., Cormier, D., Lebouteiller, V., et al. 2014, A&A, 568, A62
Di Mascolo, L., Saro, A., Mroczkowski, T., et al. 2023, Nature, 615, 809
Díaz-Santos, T., Armus, L., Charmandaris, V., et al. 2017, ApJ, 846, 32
Draine, B. T. 2011, Physics of the Interstellar and Intergalactic Medium (Princeton University Press)
Emonts, B. H. C., Lehnert, M. D., Dannerbauer, H., et al. 2018, MNRAS, 477, L60
Emonts, B. H. C., Lehnert, M. D., Yoon, I., et al. 2023, Science, 379, 1323
Ferkinhoff, C., Hailey-Dunsheath, S., Nikola, T., et al. 2010, ApJ, 714, L147
Ferland, G. J., Fabian, A. C., Hatch, N. A., et al. 2008, MNRAS, 386, L72
Ferland, G. J., Fabian, A. C., Hatch, N. A., et al. 2009, MNRAS, 392, 1475
Ferland, G. J., Chatzikos, M., Guzmán, F., et al. 2017, Rev. Mex. Astron. Astrofis., 53, 385
Fernández-Ontiveros, J. A., Spinoglio, L., Pereira-Santaella, M., et al. 2016, ApJS, 226, 19
Fujimoto, S., Ouchi, M., Ferrara, A., et al. 2019, ApJ, 887, 107
Fujimoto, S., Ouchi, M., Nakajima, N., et al. 2024, ApJ, 964, 1
Ginolfi, M., Jones, G. C., Béthermin, M., et al. 2020, A&A, 633, A90
Gullberg, B., De Breuck, C., Vieira, J. D., et al. 2015, MNRAS, 449, 2883
Harikane, Y., Ouchi, M., Inoue, A. K., et al. 2020, ApJ, 896, 93
Harikane, Y., Sanders, R. L., Ellis, R., et al. 2025, ApJ, submitted [arXiv:2505.09186]
Harrington, K. C., Vishwas, A., Weiß, A., et al. 2019, MNRAS, 488, 1489
Hill, R., Chapman, S., Scott, D., et al. 2020, MNRAS, 495, 3124
Hill, R., Chapman, S., Phadke, K. A., et al. 2022, MNRAS, 512, 4352
Kepley, A. A., Tsutsumi, T., Brogan, C. L., et al. 2020, PASP, 132, 024505
Kim, K.-T., & Koo, B.-C. 2001, ApJ, 549, 979
Klein, B., Philipp, S. D., Krämer, I., et al. 2006, A&A, 454, L29
Klein, T., Ciechanowicz, M., Leinz, C., et al. 2014, IEEE Trans. Terahertz Sci. Technol., 4, 588
Kreysa, E., Bertoldi, F., Gemuend, H.-P., et al. 2003, in Millimeter and Submillimeter Detectors for Astronomy, eds. T. G. Phillips, & J. Zmuidzinas, SPIE Conf. Ser., 4855, 41
Krumholz, M., & McKee, C. F. 2005, ApJ, 630, 250
Lagache, G., Cousin, M., & Chatzikos, M. 2018, A&A, 609, A130
Lambert-Huyghe, A., Madden, S. C., Lebouteiller, V., et al. 2022, A&A, 666, A112
Leitherer, C., Schaerer, D., Goldader, J. D., et al. 1999, ApJS, 123, 3
Lim, J., Dinh-V-Trung, Vrtilek, J., David, L. P., & Forman, W. 2017, ApJ, 850, 31
Madden, S. C., Rémy-Ruyer, A., Galametz, M., et al. 2013, PASP, 125, 600
Martins, F., Schaerer, D., & Hillier, D. J. 2005, A&A, 436, 1049
Maud, L. T., Asaki, Y., Fomalont, E. B., et al. 2020, ApJS, 250, 18
Maud, L. T., Asaki, Y., Dent, W. R. F., et al. 2022, ApJS, 259, 10
Maud, L. T., Asaki, Y., Nagai, H., et al. 2023, ApJS, 267, 24
McMullin, J. P., Waters, B., Schiebel, D., Young, W., & Golap, K. 2007, in Astronomical Data Analysis Software and Systems XVI, eds. R. A. Shaw, F. Hill, & D. J. Bell, ASP Conf. Ser., 376, 127
Meledin, D., Lapkin, I., Fredrixon, M., et al. 2022, A&A, 668, A2
Miller, T. B., Chapman, S. C., Aravena, M., et al. 2018, Nature, 556, 469
Mocanu, L. M., Crawford, T. M., Vieira, J. D., et al. 2013, ApJ, 779, 61
Mroczkowski, T., Gallardo, P. A., Timpe, M., et al. 2025, A&A, 694, A142
Muders, D., Hafok, H., Wyrowski, F., et al. 2006, A&A, 454, L25
Overzier, R. A. 2016, A&ARv, 24, 14
Papadopoulos, P., Isaak, K., & van der Werf, P. P. 2010, ApJ, 711, 757
Papadopoulos, P. P., Thi, W.-F., Miniati, F., & Serena, V. 2011, MNRAS, 414, 1705
Papadopoulos, P. P., Zhang, Z.-Y., Xilouris, E. M., et al. 2014, ApJ, 788, 153
Papadopoulos, P. P., Bisbas, T. G., & Zhang, Z.-Y. 2018, MNRAS, 478, 1716
Peng, B., Arrigoni Battaia, F., Vishwas, A., et al. 2025, A&A, 694, L1
Scoville, N., Murchikova, L., Walter, F., et al. 2017, ApJ, 836, 66
Shah, E. A., Lemaux, B. C., Forrest, B., et al. 2024, A&A, submitted [arXiv:2409.02996]
Siringo, G., Kreysa, E., Kovács, A., et al. 2009, A&A, 497, 945
Solimano, M., González-López, J., Aravena, M., et al. 2025, A&A, 693, A70
Solomon, P. M., & Vanden Bout, P. A. 2005, ARA&A, 43, 677
Spinoglio, L., Dasyra, K. M., Franceschini, A., et al. 2012, ApJ, 745, 171
Stacey, G. J., Hailey-Dunsheath, S., Ferkinhoff, C., et al. 2010, ApJ, 724, 957
Strandet, M. L., Weiss, A., Vieira, J. D., et al. 2016, ApJ, 822, 80
Uzawa, Y., Fujii, Y., Gonzalez, A., et al. 2013, Phys. C Supercond., 494, 189
Vallini, L., Gallerani, S., Ferrara, A., Pallottini, A., & Yue, B. 2015, ApJ, 813, 36
Vallini, L., Ferrara, A., Pallottini, A., & Gallerani, S. 2017, MNRAS, 467, 1300
Vieira, J. D., Crawford, T. M., Switzer, E. R., et al. 2010, ApJ, 719, 763
Vishwas, A., Ferkinhoff, C., Nikola, T., et al. 2018, ApJ, 856, 174
Vito, F., Brandt, W. N., Comastri, A., et al. 2024, A&A, 689, A130
Zhou, D., Chapman, S. C., Sulzenauer, N., et al. 2025, ApJ, 982, L17

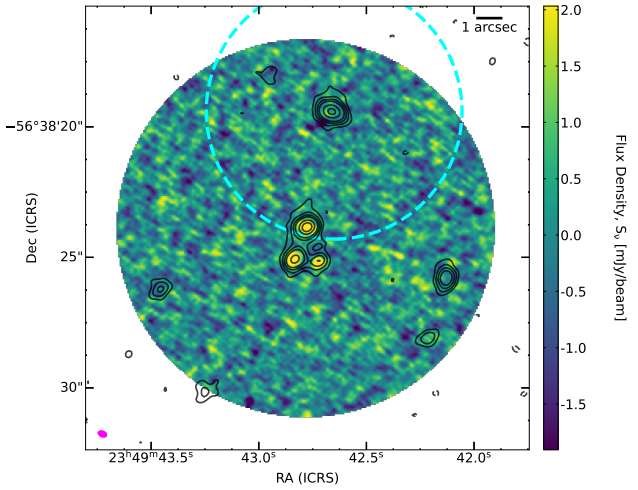

Fig. A.1. The ALMA band 10 continuum image of the Core region imaged beyond the primary beam of ~7" to explore emission from bright sources (B10 synthesized beam (magenta) shown in the bottom left corner). The APEX measurement of the [OIII] emission line comes from the cyan circle. Black contours show the band 6 dust continuum detections at signal-to-noise ratio levels of -3,3,6,10,15.

Table A.1. ALMA Band 10 continuum detections

Object name	RA J2000	DEC J2000	Flux density mJy
C3	23:49:42.774	-56:38:23.875	8.5 ± 0.8
C6	23:49:42.837	-56:38:25.070	7.0 ± 0.8
C13	23:49:42.719	-56:38:25.246	3.7 ± 0.6

Notes. The aperture based photometry used a circular diameter centered on the known positions ('Object Name' from Hill et al. 2020). A 0.7″ diameter was used for both C3 and C6, and a 0.54″ diameter aperture was used for C13. All other objects have 3σ upper limits of ~2 mJy beam^{-1}.

Appendix A: ALMA band 6 and 10 continuum

The band 10 ALMA receiver is a dual-sideband receiver that requires 90 degrees Walsh switching to split the sidebands and corresponding spectral windows in order to maximize the continuum bandwidth to ~ 8 GHz (Maud et al. 2022, 2023). This dataset was observed using the band-to-band calibration method of observing a differential gain calibrator at a lower frequency than the high frequency tuning in order to scale the higher signal-to-noise solutions to higher frequencies before eventually applying to the target source (Asaki et al. 2020a,b, 2023; Maud et al. 2020, 2022, 2023). The array configuration for band 10 reaches a field of view of ~7", maximum recoverable scale of ~3.2" and synthesized beam θ ~0.19" with Briggs weighting and a robust parameter of 0.5. For the archival ALMA band 6 data, the synthesised beam (with Briggs robust weighting factor = 0.5) is θ ~ 0.45". The field of view is 25", with a maximum recoverable scale of ~6.5".

Appendix B: Novel APEX observations compared with LABOCA sub-mm maps

APEX spectral line pointed observations used wobbler switching, which only chops in Azumith, with a 1.5 Hz rate and off-

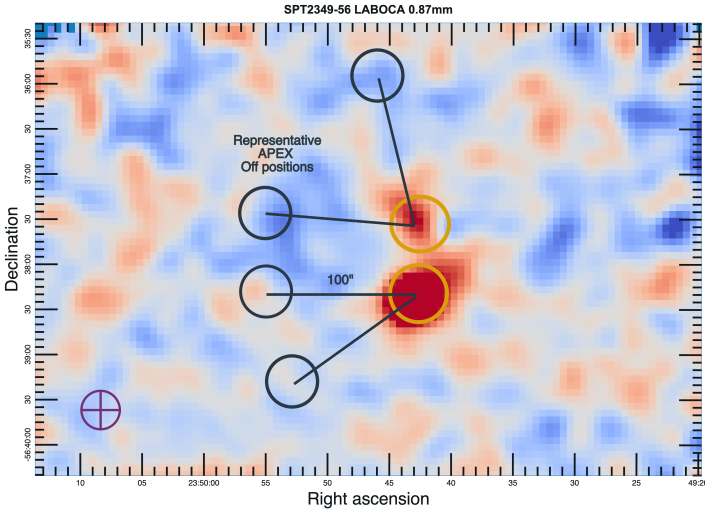

Fig. B.1. Representative 'off' positions (black circles) are shown for the APEX/SEPIA observations of the Core and North (orange circles), overlaid on LABOCA submm continuum emission (magenta beam shown in bottom left).

set of 50". Each scan consisted of a hot/sky/cold calibration, followed by up to 10 subscans of 20 s per on-source integration time. Wobbler-switching spectral line focus observations were performed every 2-4 hr and pointing checks every 1-3 hr, depending on frequency, using planets (Mars, Saturn) or standard APEX calibrators (e.g. 'pi1-Gru', 'R-Dor', 'IRAS15194-5115'). The central position for the wobbler-switching is set to an amplitude of 50", which results in an off position that is 100" from the target, as shown in the Fig B.1. A representative set of 'off' positions is shown for the APEX/SEPIA observations with respect to APEX LABOCA submm continuum maps (Hill et al. 2020).

Our result independently verifies the APEX total power measurements first reported by Strandet et al. (2016), and recently highlighted by Zhou et al. (2025) in the context of excess CO(4-3) emission. We note that the pointing in Strandet et al. (2016) was identical as ours, and still agrees with our novel measurements of the Core using SEPIA345 with better receiver baseline stability. This consistency between measurements remains despite using a completely different instrument (i.e. the decommissioned FLASH instrument (Klein et al. 2014), with the observations in Strandet et al. (2016) having taken place before the complete refurbishment of the primary mirror for APEX in 2017.

If we consider the global dust emitting region, previous LABOCA measurements had measured more 870 μm flux density than reported with ALMA (Miller et al. 2018; Hill et al. 2020). The elongated structure that extends to the North is where we find a relative excess of 4× amount of [CII] emitting gas compared to the one galaxy, yet extended dust from LABOCA is likely diffuse, warm and optically thin. We therefore consider dust attenuation of the [OIII] line from any large-scale dust emission to be negligible. Still, this suggests there could be additional line emission that are resolved out by interferometers like ALMA.